

pubs.acs.org/crystal Article

Band Structure Engineering Based on InGaN/ZnGeN₂ Heterostructure Quantum Wells for Visible Light Emitters

Md Rezaul Karim, Benthara Hewage Dinushi Jayatunga, Kaitian Zhang, Menglin Zhu, Jinwoo Hwang, Kathleen Kash, and Hongping Zhao*



Cite This: Cryst. Growth Des. 2022, 22, 131–139

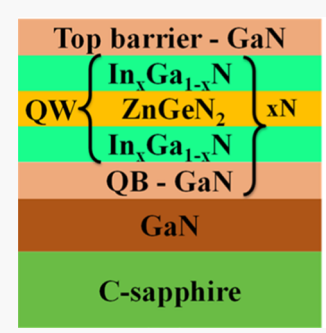


ACCESS

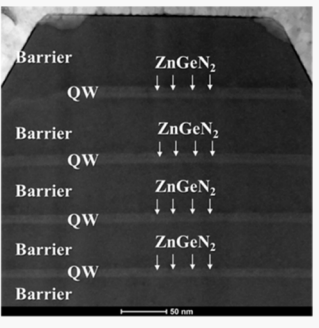








MOCVD development of InGaN-ZnGeN₂ QWs for lightemitting diodes



ABSTRACT: Band structure engineering based on InGaN/ZnGeN₂ heterostructure quantum wells (QWs) is proposed to address the long-standing charge separation challenge in visible light emitters using polar InGaN QWs as active media. A nanometer-scale layer of ZnGeN₂ is successfully incorporated in InGaN QWs via metalorganic chemical vapor deposition. Understanding the structural properties of the heterostructure QWs reveals that the growth conditions for the GaN barrier layers play an important role in the QW properties. Specifically, the structural quality of the QWs is improved by increasing the thickness and the growth temperature of the GaN barrier layers. Due to the large band offset at the InGaN/ZnGeN₂ heterointerface, the position and thickness of the ZnGeN₂ sub-layer within the InGaN QWs determine the potential minima and thus the carrier wave functions in both conduction and valence bands. This work demonstrates the effectiveness of emission wavelength tunability of InGaN/ZnGeN₂/InGaN heterostructure QWs via tuning of the ZnGeN₂ sub-layer properties. More significantly, the peak emission of InGaN/ZnGeN₂/InGaN heterostructure QWs can be extended to longer wavelengths without increasing the In composition or the QW thickness. Results from this work provide a new route for addressing the low quantum efficiency of conventional InGaN QWs emitting at green and longer wavelengths.

1. INTRODUCTION

An external quantum efficiency (EQE) greater than 80% has already been achieved in III-N-based blue light emitting diodes (LEDs), and an EQE greater than 60% has been achieved in III-P-based red LEDs.¹ Unfortunately, the EQEs of the state-of-the-art green and amber LEDs are only 44% and 18%, respectively.¹ The direct-to-indirect band gap cross-over of the AlGaInP material system, at slightly over 2.3 eV, fundamentally limits the achievable EQE in III-P based amber, green, and blue LEDs.² The InGaN material system has a direct band gap over the entire visible spectrum and is considered to be a more viable option for developing high efficiency green and amber LEDs.²

One of the major challenges in InGaN quantum well (QW)-based LEDs is associated with the polarization-induced internal electric field, which bends the energy bands and creates a separation between the electron and hole wave functions. ^{2,3} A reduction in the electron—hole wave function overlap causes the radiative recombination rate to decrease and, hence, the

quantum efficiency to drop. This phenomenon is known as the quantum-confined Stark effect (QCSE).³ In addition, the miscibility gap between GaN and InN leads to random alloy fluctuations and phase segregation in high-In-content InGaN, which increases the density of nonradiative recombination centers (NRCs).^{3,4} The growth of high-In-content InGaN requires a low growth temperature, which further deteriorates the crystalline quality and in turn increases the density of NRCs. The severity of all of these adverse phenomena increases with the increase in either the In content or the width of the QW, either or both of which are necessary for extending the emission wavelength into green, amber, and red.³

Received: June 1, 2021
Revised: November 12, 2021
Published: November 22, 2021





To reduce or eliminate the internal field-induced charge separation, InGaN QWs grown along the nonpolar m-axis or the semipolar a-axis have been investigated extensively both theoretically and experimentally.⁵⁻⁷ However, the unavailability of large-size inexpensive free-standing m-plane or aplane GaN and the large density of extended defects in heteroepitaxial m-plane or a-plane GaN on foreign substrates limit the development of nonpolar or semipolar InGaN QWs. Another approach to mitigate the QCSE is to engineer the band structure of the InGaN QWs grown along the polar cplane to increase the overlap between the electron and hole wave functions.⁸ Previously proposed band structure engineering solutions for III-nitride QWs include staggered InGaN QWs, 8-12 strain-compensated InGaN/AlGaN QWs, 13,14 InGaN/δ-InN QWs,¹⁵ and type-II InGaN/GaNAs QWs,^{16,17} all of which have shown enhancement of the electron-hole wave function overlap. However, the In content required in these structures for green and longer emission wavelengths remains problematically high.8

Recently, the use of a hole confinement layer to overcome the QCSE in visible ^{18,19} and ultraviolet²⁰ wavelength emitting III-nitride QWs has been investigated theoretically. The calculated electron-hole wave function overlaps have shown two- to threefold enhancement in blue- and green-emitting InGaN/ZnGeN₂/InGaN QWs compared to those of the conventional InGaN QWs designed for the same peak emission wavelengths. 18 Another advantage of the InGaN/ ZnGeN2/InGaN QW over the conventional QW is the reduction in the required In content to achieve a targeted peak emission wavelength. The band gap and lattice constant of ZnGeN₂ are similar to those of GaN.^{21–24} These two materials form a type-II heterostructure in which the valence band of ZnGeN₂ lies more than 1 eV above that of GaN.^{25–27} Due to the large valence band offset, the ZnGeN2 sub-layer in an InGaN/ZnGeN₂/InGaN QW provides strong hole confinement, which in turn enhances the electron-hole wave function overlap.

There has been no experimental report on the implementation of InGaN/ZnGeN₂/InGaN heterostructure QWs. Recently, we reported the development of metalorganic chemical vapor deposition (MOCVD) of ZnGeN2 on GaN-on-sapphire templates²⁸ and sapphire substrates.²⁹ The band offsets between GaN and ZnGeN₂ were determined experimentally.²⁷ In this paper, MOCVD growths of InGaN/ZnGeN₂/InGaN QWs on GaN templates were investigated. The effects of the thicknesses and growth temperatures of the GaN barrier layers on the structural properties of the QWs were studied. The smoothness of the InGaN/ZnGeN2/InGaN QWs improved with increasing both the thickness of the GaN barrier and the barrier growth temperature. The effects of the thickness and position of the ZnGeN₂ layer within the InGaN QWs on the optical properties of the InGaN/ZnGeN₂/InGaN heterostructure QWs were characterized using cathodoluminescence (CL) and photoluminescence (PL) spectroscopy measurements. The emission efficiencies of the QWs were observed to depend on the ZnGeN2 layer growth temperature and thickness. The peak wavelengths were observed to depend on the ZnGeN2 layer thickness and its location within the InGaN QW. For higher growth temperatures, the PL and CL spectra showed the emergence of a new peak, which was not present in the spectra of the conventional InGaN QWs. This new peak is attributed to Zn defect levels.

2. Experimental Details. Figure 1a,b shows the schematic of the conventional InGaN QWs with GaN barriers and the

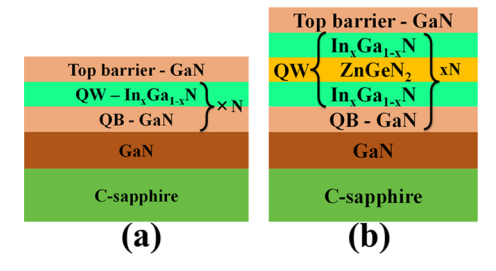


Figure 1. Schematic design of (a) conventional GaN/InGaN/GaN QWs and (b) $GaN/(InGaN/ZnGeN_2/InGaN)/GaN$ QWs. N is the number of QWs in the samples.

InGaN/ZnGeN2/InGaN QWs grown in this work. The conventional QWs consist of single InGaN layers, whereas the heterostructure QWs consist of InGaN/ZnGeN2/InGaN QW layers with the same GaN barriers. The samples were grown on GaN-on-sapphire templates via MOCVD. The HVPE-grown GaN templates used in this study were commercially purchased. The growths were initiated by regrowth of a 150-200 nm thick GaN layer at 975 °C and 200 Torr reactor pressure. Trimethylgallium (TMGa) and ammonia (NH₃) were used as the precursors of Ga and N, respectively, and H₂ was used as the carrier gas for this layer. The temperature was then ramped down to 700 °C, and the pressure increased to 500 Torr to grow an InGaN/GaN superlattice (SL) layer. Next, the multiple QWs (MQWs) were grown on top of the SL layer, using triethylgallium (TEGa), trimethylindium (TMIn), and NH3 as the precursors for Ga, In, and N, respectively, while N₂ was used as the carrier gas. The ZnGeN₂ sub-layers in these samples were grown using diethylzinc (DEZn), germane (GeH₄), and NH₃ as the precursors for Zn, Ge, and N, respectively, with N₂ as the carrier gas. The growth conditions for the barrier and QW layers are listed in Table 1. A quotation mark in the table indicates that the value listed is the same as the one above it, and is used to help highlight similarities and differences among the growth conditions for the different samples. All the layers were grown in the same chamber without interruption. While the samples are labeled A through M for the purpose of discussion of the results presented here, the table also lists the run numbers, which are used to catalogue the sample library. The results presented here are representative of the findings from over 200 QW growth runs.

The structural properties of the samples were investigated via X-ray diffraction (XRD) using a Bruker ADVANCED D8 Discover XRD and scanning transmission electron microscopy (STEM) using a Thermo Fisher Titan STEM operated at 300 kV. The elemental compositions along the cross sections of the samples were determined using energy-dispersive X-ray spectroscopy (EDS) measurements. CL measurements were performed using a Thermo Fisher Quattro environmental scanning electron microscope equipped with a Horiba H-Clue CL detector. A 325 nm wavelength cw He–Cd laser was used as the excitation source for the PL measurements. The excitation spot size was approximately 100 μ m in diameter. The excitation power used was approximately 0.50 mW.

3. Results and Discussion. The successful insertion of a ZnGeN₂ sub-layer in between two InGaN layers was confirmed by STEM imaging and EDS line scans along the cross sections

Table 1. Growth Run Number, Number of Quantum Wells, Ammonia (NH₃) Flow Rate in sLm, Chamber Pressure in Torr, Barrier and Well Growth Temperatures (T) in °C, Triethylgallium (TEGa), Trimethylindium (TMIn), Diethylzinc (DEZn), and Germane (GeH₄) Flow Rates in μ mol/min, and Duration (t) in sec for the GaN Barrier and InGaN/ZnGeN2/InGaN Quantum Well Layers

		t (sec)	5.0	4.0				5.0		3.5	5.0	7.0	3.5		
InGaN well	ZnGeN ₂ layer	DEZn (μ mol/min) GeH ₄ (μ mol/min) t (sec)	5.3											layer	layer
			190	159		106	159	340						no ZnGeN2 layer	no ZnGeN ₂ layer
	t (sec)	above ZGN	40	25				09	06	20			32		
		below ZGN	40	20				09	06	30			18	06	20
	TMIn	$(^{\circ}C)$ $(\mu mol/min)$ $(\mu mol/min)$ below ZGN above ZGN	8	17				23		8				23	∞
	TEGa	(µmol/min)	6					7		6				7	6
	T	(°C)	009	200		029	200	089		735				089	735
	GaN barrier	t (sec)	230	808	205	089	150	006		230				006	230
		TEGa (µmol/min)	6					10		6				10	6
		(°C)	009	780		0/9	200	780		735				780	735
		P (Torr)	200					400		200				400	200
	3					4		3				4	е		
$\label{eq:controller} \text{GaN barrier}$ QW run # # of QWs NH3 (sLm) P (Torr) T (°C) TEGa (μ mol/min) t (sec)			3					4		3				4	3
			87	228	229	226	198	30	29	86	95	26	100	27	92
sample C			¥	В	С	О	Э	ц	Ü	Н	Ι	Ĺ	X	Г	М

of the samples. The middle panel shown in Figure 2 shows the cross-sectional STEM image of the InGaN/ZnGeN₂/InGaN QW sample A, whereas the left panel shows the corresponding schematic design. The GaN barrier layer and the InGaN and ZnGeN₂ layers in the well region are marked by the red arrows. The GaN, InGaN, and ZnGeN2 layers are clearly noticeable from the contrast difference in the STEM image. The right panel shown in Figure 2 shows the atomic fractions of Ga, In, and Zn determined from the EDS scan along the vertical direction on the STEM image in the middle panel. The position of the peak in the Zn concentration profile, which coincides with the dips in the In and Ga profiles, aligns with the position of the ZnGeN2 layer in the STEM image, confirming the successful implementation of InGaN/ZnGeN₂/ InGaN QWs with GaN barriers. Based on the EDS line scans, the In composition in the InGaN layers was ~10 at. %.

3.1. Effects of Barrier Growth Temperature and Barrier Thickness on InGaN/ZnGeN2/InGaN QW Structures. A series of samples was grown to investigate the effects of barrier thickness and barrier growth temperature on the structure of the InGaN/ZnGeN₂/InGaN QWs. Figure 3 shows the XRD 2θ - ω scan profiles of the two InGaN/ZnGeN₂/ InGaN QW samples B and C. These two samples were grown using identical conditions except with different targeted thicknesses of the GaN barrier layers-30 and 12 nm, respectively. For both samples, a growth temperature of 780 °C was used for the GaN barrier layers, whereas 700 °C was used for the InGaN and the ZnGeN2 layers. Based on the EDS line scan of sample E, for which the process conditions for the InGaN layers were the same as those used for these samples. the In compositions in the InGaN layers in samples B and C are \sim 6.5 at. %. For both samples, the XRD 2θ - ω scan profiles show satellite peaks on both sides of the GaN (0002) peak; these are attributed to the QW structures. The peak at $2\theta \sim$ 33.1° corresponds to the metallic In residual. The peak at 35.8° is assigned to the (0002) peak of the buffer AlGaN layer in the GaN/c-sapphire template. The position of the AlGaN (0002) peak was observed to vary from template to template, probably due to variations in Al composition in the buffer layers from wafer to wafer.

For sample B (black curve, barrier thickness \sim 30 nm), the XRD 2θ - ω scan profile shows several well-resolved peaks, indicative of high structural quality, thickness uniformity, and sharp interfaces for the QWs. In contrast, the peaks in the XRD 2θ - ω scan profile of sample C (red curve, barrier thickness \sim 12 nm) are not nearly as well resolved, indicating a degraded structural quality (e.g., inhomogeneous thickness and/or In composition) of the QWs in this sample, compared to sample B. This qualitative XRD result demonstrates that the thicker barrier of sample B results in improved QW structural quality. The mechanism of this dependence of the structural quality of the GaN/InGaN/ZnGeN₂/InGaN/GaN QWs on the GaN barrier thickness is not yet well understood, and its investigation is a work in progress.

To investigate the effects of the GaN barrier growth temperature on the structural quality of the InGaN/ZnGeN₂/InGaN QWs, two additional samples (D and E) are compared with samples B and C. The targeted barrier thicknesses of B and D were both \sim 30 nm. In Figure 4a, the XRD 2θ - ω scan profile of sample D shows only three resolved satellite peaks, compared to eight for sample B. The major differences are the barrier and QW growth temperatures for the two samples. These were 780 and 700 °C for the barriers

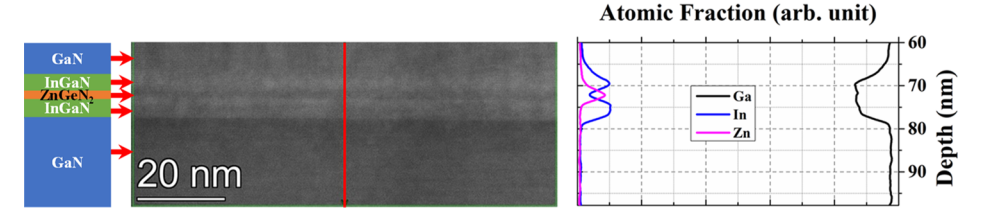


Figure 2. Cross-sectional STEM imaging of InGaN/ZnGeN₂/InGaN QW sample A (center panel), the schematic of the structure (left panel), and the atomic fraction of Ga, In, and Zn along the vertical direction (averaged over the scanning area) shown in the center panel determined from the EDS scan.

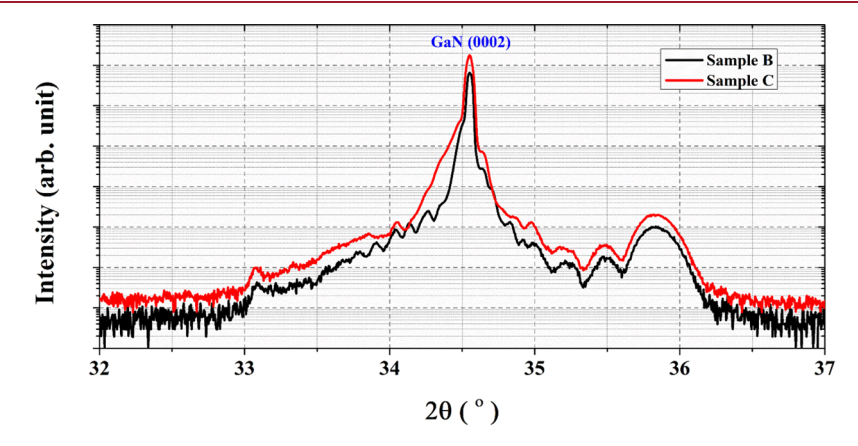
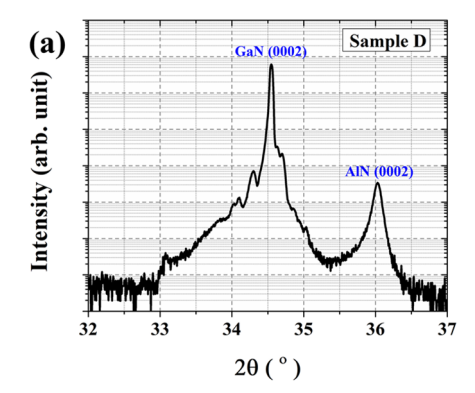


Figure 3. XRD 2θ - ω scan profiles of InGaN/ZnGeN₂/InGaN QW samples B and C. The targeted GaN barrier thicknesses were 30 and 10 nm, respectively. The peak at $2\theta \sim 33.1^{\circ}$ is attributed to residual In on the surface. The peak at $2\theta \sim 35.7^{\circ}$ corresponds to the AlGaN buffer layer in the GaN/c-sapphire template.



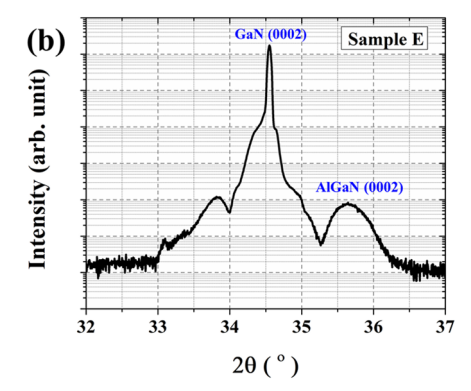


Figure 4. XRD 2θ - ω scan profiles of InGaN/ZnGeN₂/InGaN QWs (a) sample D and (b) sample E. The targeted GaN barrier thicknesses in samples D and E were 40 and 10 nm, respectively.

and QWs for sample B, respectively, and 670 °C for both, for sample D. The In composition in the InGaN layers in sample

D is estimated to be 13 at. %, which is obtained from STEM EDS.

Samples C and E have similar barrier thicknesses at \sim 12 nm for C and \sim 10 nm for E. The parameters for these two growth runs were otherwise identical except for the barrier growth temperature, which was 780 °C for sample C and 700 °C for sample E. The XRD 2θ - ω scan profile of sample E, shown in Figure 4b, has only one broad satellite peak on the left of the InGaN zeroth order peak. The separation between the superlattice peak and the InGaN zeroth order peak for sample E is larger than that for samples B and C. The XRD data clearly show lower structural quality for samples D and E as compared to samples B and C. We attribute this lower structural quality to the lower growth temperatures and lower thicknesses of the GaN barrier layers.

Figure 5a shows the cross-sectional STEM image of an InGaN/ZnGeN₂/InGaN QW sample F. The growth temperatures of the GaN barrier layers and the InGaN/ZnGeN₂/InGaN QW layers were 780 and 680 °C, respectively. The STEM image shows well-defined QW structures with four periods. The ZnGeN₂ layers sandwiched between the two InGaN layers are clearly visible in each of the periods. The GaN and InGaN layers are marked as the barrier and well, respectively. The ZnGeN₂ layers are marked by the downward white arrows. The total thickness of the InGaN/ZnGeN₂/InGaN heterostructures is approximately 10.5 nm, and the barriers are ~50 nm thick. Figure 5b shows the XRD 2θ - ω scan profile of sample F. The well-resolved satellite peaks in the XRD 2θ - ω scan profile further confirm the high structural quality of the sample.

The center panel shown in Figure 6 shows the cross-sectional STEM image of sample E. The left panel shows the design of the targeted structure for this growth. For this

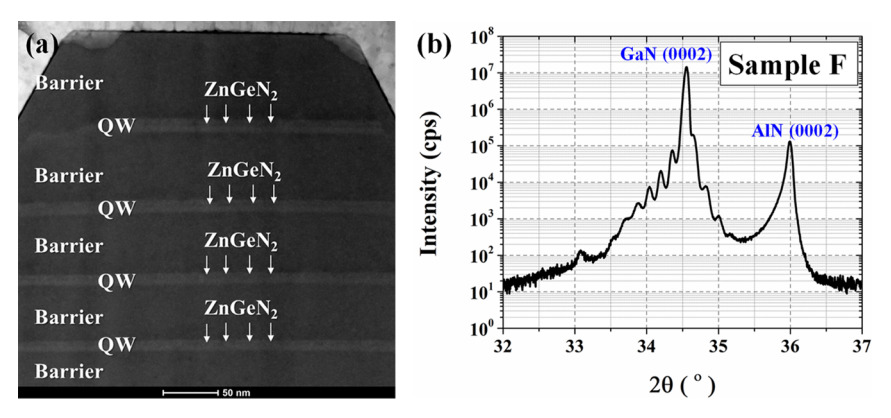


Figure 5. (a) Cross-sectional STEM imaging of the four-period InGaN/ZnGeN₂/InGaN QW sample F. The GaN and InGaN layers are marked as "barrier" and "QW", respectively. The ZnGeN₂ layers are marked by downward white arrows. (b) XRD 2θ - ω scan profile of sample F.

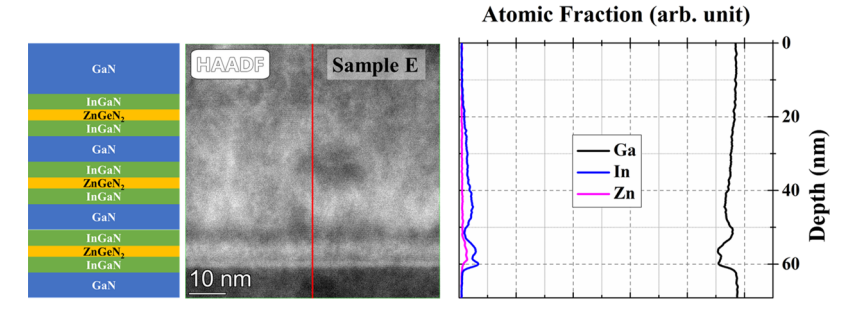


Figure 6. Cross-sectional STEM imaging of InGaN/ZnGeN₂/InGaN QW sample E (center panel), a schematic design of the intended sample from this growth (left panel), and atomic fractions of Ga, In, and Zn (right panel) determined from EDS scans along the vertical direction (averaged over the scanning area) on the STEM image. The left panel shows the design of the intended structure from this growth.

sample, a growth temperature of 700 °C was used for both the GaN barrier and InGaN/ZnGeN2/InGaN well layers, with a barrier thickness of ~10 nm. Despite the fact that the growth was programmed for three periods of InGaN/ZnGeN₂/InGaN QWs with GaN barriers, only the first period (with an In composition of 6.5 at. %) can be identified in the STEM image. The region above the first QW appears to be a continuous InGaN layer, probably a result of severe In diffusion into the GaN barrier layers. The EDS scan measured along the vertical direction on the cross-sectional STEM image in the center panel shows a peak in the Zn profile that coincides with the dip in the In profile in the first QW. For the subsequent QWs, the In profile peaks approximately around the designed center of the middle QW and gradually decreases to the background composition over a thickness of ~35 nm. Based on the XRD 2θ - ω scan profiles and the cross-sectional STEM images shown in Figure 3 through Figure 6, we conclude that relatively higher barrier growth temperatures and thicker barriers are necessary in order to maintain the high structural quality of the GaN/ (InGaN/ZnGeN₂/InGaN)/GaN MOWs.

3.2. Effects of the Position and Thickness of the ZnGeN₂ Layers on the Optical Properties of the InGaN/ZnGeN₂/InGaN QWs. In Figure 7, the room-temperature CL spectra of InGaN/ZnGeN₂/InGaN QW sample G are plotted along with the spectrum of a conventional InGaN QW sample L. The inset shows the same spectra but normalized with respect to the corresponding maximum intensities. The growth conditions used for the GaN barrier and InGaN well layers were the same for samples G and L. In the CL spectrum of the conventional InGaN QW sample L, the peak at 400 nm corresponds to the band-to-band emission peak from the InGaN well layers. The shoulder at ~470 nm can be attributed

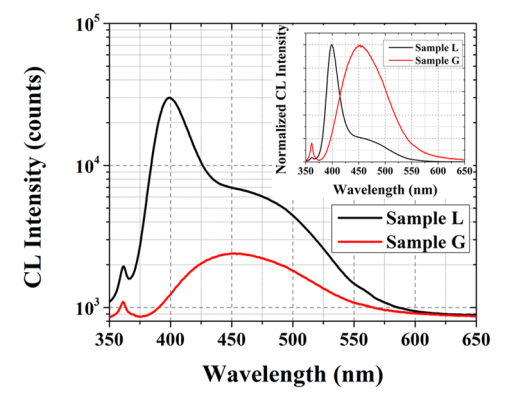


Figure 7. Room-temperature CL spectra of $InGaN/ZnGeN_2/InGaN$ QW sample G along with that of the reference InGaN QW sample L. The beam acceleration voltage and electron beam current were set to 5 kV and 0.71 nA, respectively.

to a defect-related emission band. We have grown a series of conventional InGaN QW samples and have observed that the defect band is at $\sim 0.3-0.5$ eV lower energy position, compared to the band-to-band emission peak. Both peaks shift to lower energy with an increase in the In content of the InGaN layer. These results are consistent with previously reported results for the Zn-related emission band in InGaN QWs. 31,32

For the InGaN/ZnGeN₂/InGaN QW sample G, the peak intensity of the CL spectrum shown in Figure 7 is lower than that of the reference InGaN QW sample L by more than 1 order of magnitude. This reduction in PL efficiency is probably a result of structural degradation in the QW, for example, due

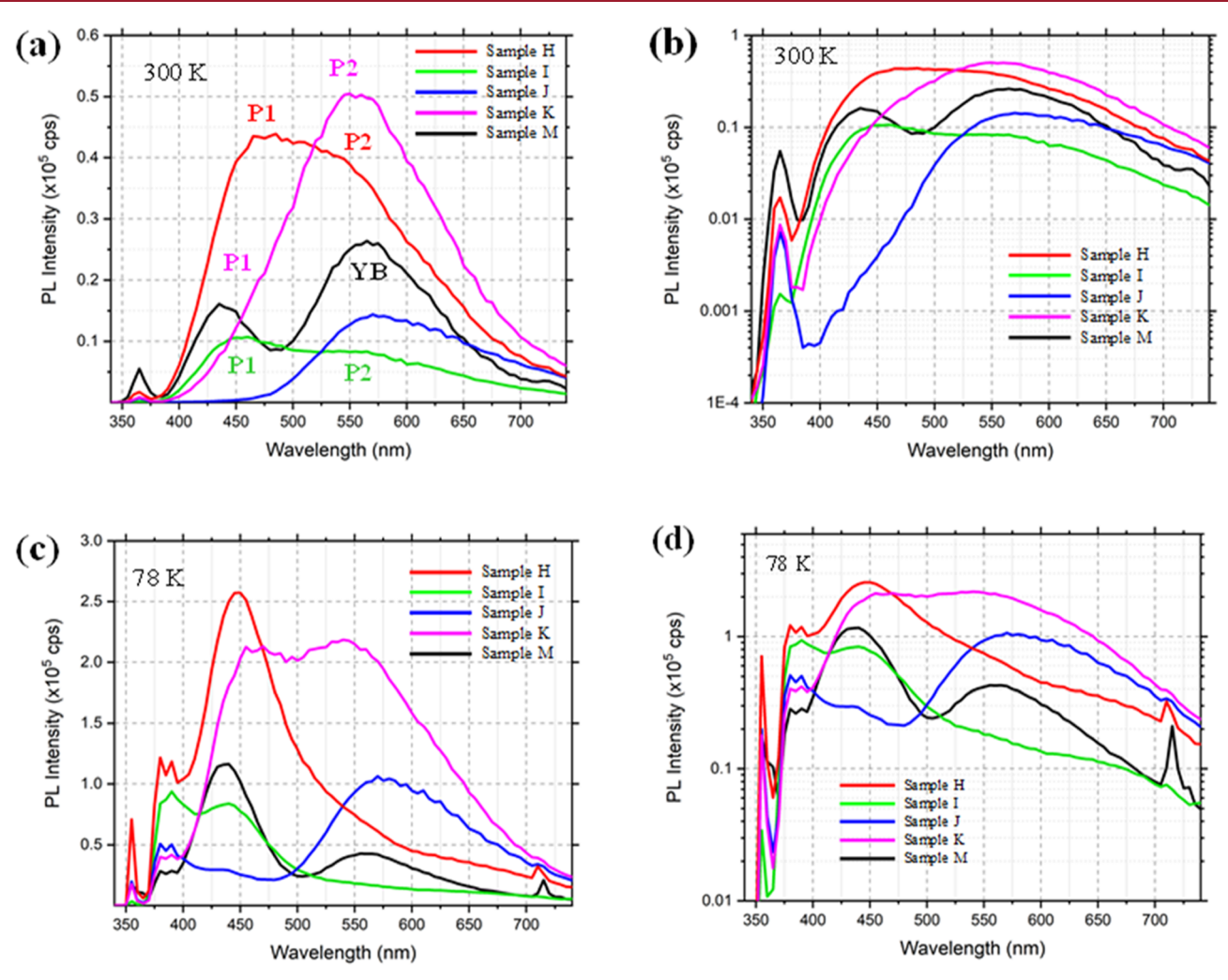


Figure 8. PL spectra of InGaN/ZnGeN₂/InGaN QW samples H, I, J, and K and the reference InGaN QW sample M at 300 K in linear scale (a) and in semilog scale (b) and at 78 K in linear scale (c) and in semilog scale (d) 325 nm He–Cd laser was used as the excitation source.

to an increase in the interfacial roughness and/or a higher density of extended defects, which act as NRCs, resulting from the insertion of the ZnGeN2 layers. It has been shown that the density of extended defects in ZnGeN2 decreases with the increase in growth temperature in the range of 600-770 °C. The ZnGeN₂ layer in sample G was grown at 680 °C. An increase in the growth temperature of the InGaN/ZnGeN₂/ InGaN well may help to improve the PL efficiency of the GaN/(InGaN/ZnGeN2/InGaN)/GaN QWs. In addition, the inset shown in Figure 7 clearly shows a red shift of the peak position and broadening of the peak for sample G, compared to the band-to-band emission peak of the reference InGaN QW sample L. 33,34 The red shift of the peak emission wavelength in the InGaN/ZnGeN2/InGaN QW structure, compared to the conventional InGaN QW structure with the identical InGaN thickness and In composition, is attributed to the band structure engineering resulting from the large band offset between InGaN and ZnGeN2, in agreement with predictions from numerical simulations.

To investigate the effects of the thickness and position of the ZnGeN₂ sub-layer on the emission properties of the InGaN/ZnGeN₂/InGaN QWs, samples H–K were grown at a temperature of 735 °C for both the barrier and well layers. A conventional InGaN QW sample M was also grown using the same conditions. The total growth duration for the two

InGaN sub-layers in a single QW period for samples H–K was equal to the growth duration of the InGaN QW in sample M. The growth durations of the InGaN sub-layers below and above the ZnGeN₂ layers in a single period were 30 s and 20 s, respectively, for samples H–J and 18 and 32 s, respectively, for sample K. The growth duration for the ZnGeN₂ sub-layer was 3.5, 5.0, 7.0, and 3.5 s for samples H, I, J, and K, respectively.

Figure 8a shows the room-temperature (300 K) PL spectra of the conventional InGaN QW sample M along with the PL spectra for the InGaN/ZnGeN₂/InGaN QW samples H–K. Figure 8b shows the same spectra but in the semilog scale. Figure 8c,d shows the linear and semilog spectra for the same samples at 78 K. All of the spectra show a near-band-edge GaN peak at 363–364 nm (3.41 eV). The 78 K spectra also show emission from shallow defect states, which are poorly resolved at the 5 nm resolution used for these spectra. Relatively narrow peaks around 730 nm wavelength observed in some of the spectra arise from the second order diffraction peaks of the GaN near-band-edge emission.

We focus now on the PL spectra of the reference sample M. The band-to-band emission peaks from the InGaN QW cannot be resolved from the near-band-edge peak of GaN at room temperature (\sim 3.41 eV) due to the low In content in the InGaN well layer, which was determined to be 0.35 at.% from the XRD 2θ - ω scan profile, as shown in Figure 10a. This

composition should yield a reduction of the band gap from that of GaN by approximately 150 meV, which should yield a band edge wavelength of 380 nm, or 3.26 eV, at 300 K. We attribute the dominant peak at approximately 435 nm (2.85 eV) at both temperatures to recombination from Zn defects in the QW. This peak is shifted down in energy from the band edge by 0.40 eV. It is approximately 0.20 eV higher in energy than the Zn-related defect peak for samples G and L, as shown in Figure 7, and thus roughly tracks the differences in the band gaps of the QWs for these two sets of samples. The wellknown, broad "yellow-band" emission peak centered at approximately 560 nm is also clear in both of the sample M spectra. This peak is associated with the GaN template, not with the QW barriers. While the Zn-related QW peak increased in intensity by a factor of approximately 7.5 on lowering the temperature from 300 to 78 K, due to the reduction in nonradiative defect recombination, the "yellow band" peak increased in intensity by only a factor of approximately 1.5.

Two peaks are also evident in the spectra of samples H through K, labeled P1 and P2 in Figure 8a. By comparison of these spectra with those of sample M, it is clear that the shorter wavelength P1 peaks, occurring at 440-445 nm, are the Znrelated defect peaks associated with the QWs. They are evident in all of these samples, either in the spectra taken at 300 K or those taken at 78 K, or both. For samples J and K, the peaks are not seen in the linear plots at 300 K, but are hinted at in the curvatures in the semilog plots of Figure 8b. At 78 K, P1 is relatively strong in sample K and also appears as a weak peak in sample J. The apparent peak positions for some samples are shifted by convolution with the second, longer wavelength peak. With deconvolution, the P1 peaks appear at approximately 440-450 nm at 78 K (see the Supporting Information). We would expect the peak positions to change with temperature by approximately 6 nm based upon the temperature dependence of the band gap of GaN. Given the widths of the observed peaks, the expected change in peak position with temperature is minor and allows for easy comparison of the peak positions at the two temperatures.

The P2 peaks for all of the samples shown in Figure 8a occur in roughly the same spectral region as the GaN "yellow band" peak for sample M. We focus first on the spectra of sample J. Here, the ZnGeN₂ layer growth time was 7 s, compared to 3.5 s for samples H and K and 5 s for sample I. The thickness of the ZnGeN₂ layer is not determined, but a roughly estimated growth rate is 600 nm/h, ²⁹ which for a 7 s growth yields a layer 1.2 nm thick—about 2.4 unit cells. The increase in recombination efficiency of P2 from 300 to 78 K is over a factor of 7, a temperature dependence that does not follow that of the "yellow band" recombination and leads us to conclude that P2 here is likely from intrinsic recombination associated with the band structure engineering accompanying the insertion of the ZnGeN₂ layer.

We turn next to the interpretation of the temperature dependence of the spectra of samples H and I. Figure 9 shows the spectra for samples H–K and M, for both temperatures, normalized with respect to the maximum peak height. We are reminded that the peaks at 380–390 nm are from recombination from defects from the GaN template layer. It is evident that carrier transfer from the states responsible for P1 to those involved in P2, in samples H and I, is suppressed at the lower temperature, in contrast to the finding for sample J. We tentatively attribute this result to the thinner ZnGeN₂

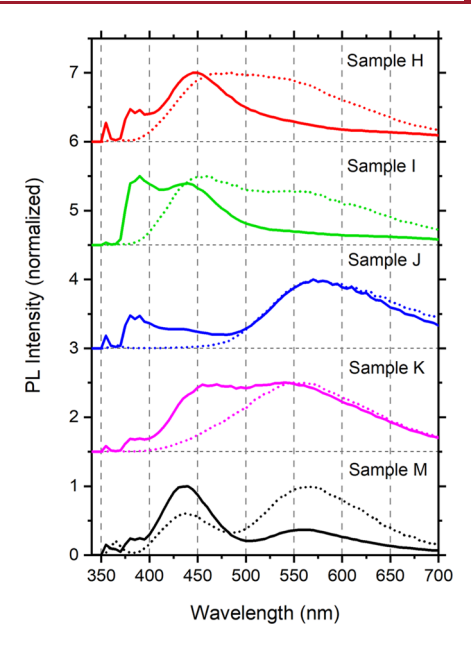


Figure 9. PL spectra of InGaN/ZnGeN $_2$ /InGaN QW samples H, I, J, and K and the reference InGaN QW sample M at 300 K and 78 K, shown normalized to emphasize the changes in relative recombination efficiencies of peaks P1 and P2 with temperature. The spectra are offset in the vertical axis for clarity. The lower, dashed line of each pair of spectra is the 300 K spectrum for that sample. The upper, solid line is the 78 K spectrum.

layers in these samples. For sample H, our rough estimate of the thickness of the $\rm ZnGeN_2$ layer is 0.6 nm, or 1.2 unit cells, and for sample I, 1.7 unit cells. It is reasonable to expect that the roughness of the interfaces will play a larger role for thinner layers and might lead to suppression of recombination via barriers to carrier transfer and carrier localization.

By contrast, the temperature dependence of sample K more resembles that of sample J, but with more efficient P1 recombination at 78 K. This sample differs from sample H in only one respect. The ZnGeN₂ sub-layer for sample K is located at about 36% of the total InGaN layer thickness, rather than at the 60% location for sample H. Recalling that the QCSE pulls the electron toward the front of the QW and the hole toward the back (i.e., farther along the growth direction), the result is that for sample K, compared to sample H, the electron—hole overlap should be increased, thus enhancing the P2 recombination efficiency and partially, though not totally, overcoming the effect of suppression of recombination at a low temperature due to layer thickness fluctuations in this thin ZnGeN₂ insertion layer.

Figure 10b shows the room-temperature CL spectra of the InGaN/ZnGeN₂/InGaN QW samples H and K along with that of the conventional InGaN QW sample M. The spectra from samples H and K show one more peak than those in the spectrum of sample M, consistent with the PL measurements. Figure 10c shows the CL spectra obtained at 79 K and 296 K on sample H. At 79 K, the intensities of both peaks increased by a factor of 2–3, but the peak P1 became dominant. The integrated CL intensity over 380–600 nm at 296 K is 47% of that at 79 K.

4. Conclusions. Band structure engineering based on InGaN/ZnGeN₂/InGaN heterostructure QWs was investigated via MOCVD. The structural properties of the QWs were probed via STEM imaging, which clearly shows thin ZnGeN₂

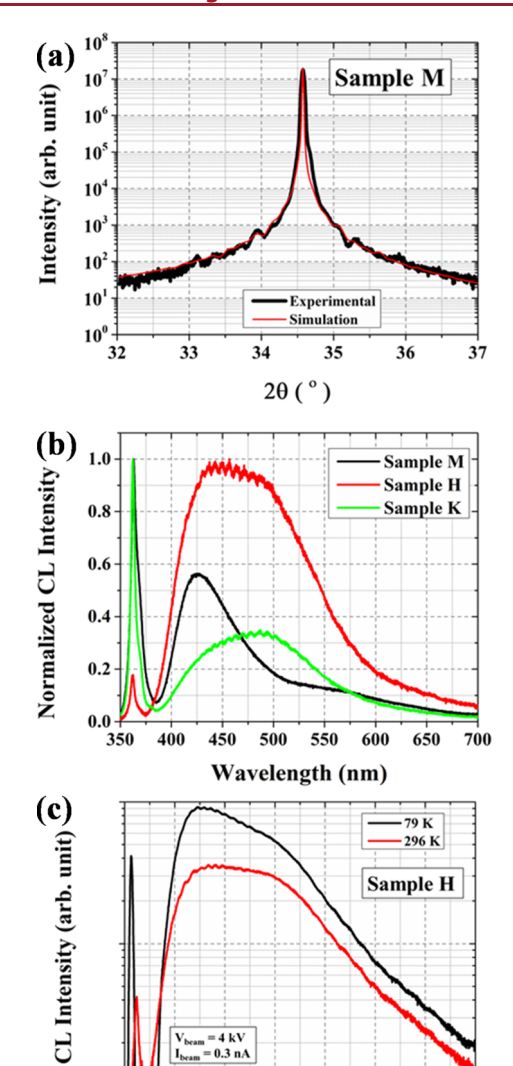


Figure 10. (a) XRD 2θ - ω scan profile of sample M. The simulated profile (red curve) was fitted over the measured profile (black curve) to determine the In content. (b) Room-temperature CL spectra of the InGaN QW sample M and InGaN/ZnGeN₂/InGaN QW samples H and K. The spectra were normalized with respect to their respective peak intensities. (c) CL spectra of sample H measured at 296 K and at 79 K.

500 550

Wavelength (nm)

400

450

350

sub-layers sandwiched between two InGaN sub-layers. The smoothness of the InGaN/ZnGeN₂/InGaN QWs improved with the increase in barrier thickness and barrier growth temperature, as measured by STEM. The emission properties of the InGaN/ZnGeN2/InGaN QW structures were investigated using CL and PL spectroscopy measurements. These measurements reveal a clear dependence of the emission efficiencies on the ZnGeN2 layer growth temperature, as well as a clear dependence of the emission efficiencies and the peak wavelengths on the thickness of the ZnGeN₂ layers. For a 680 °C QW growth temperature, the emission intensity of the InGaN/ZnGeN₂/InGaN QWs was substantially reduced as compared to the conventional InGaN QWs grown under the same conditions. For a 735 °C growth temperature, the PL and CL spectra of the InGaN/ZnGeN₂/InGaN QWs showed the emergence of a new peak, which was not present in the spectra

of the conventional InGaN QWs. Although additional experimental work is required to completely understand and control the emission properties of InGaN/ZnGeN₂/InGaN heterostructure QWs, this work is a significant step forward in the implementation of hybrid III-N, II-IV-N₂ heterostructures in nitride-based LEDs for increased efficiency in the green and longer wavelengths.

ASSOCIATED CONTENT

Supporting Information

The Supporting Information is available free of charge at https://pubs.acs.org/doi/10.1021/acs.cgd.1c00630.

Deconvolution of PL spectra (PDF)

AUTHOR INFORMATION

Corresponding Author

Hongping Zhao — Department of Electrical and Computer Engineering and Department of Materials Science and Engineering, The Ohio State University, Columbus, Ohio 43210, United States; orcid.org/0000-0002-5169-5290; Email: zhao.2592@osu.edu

Authors

Md Rezaul Karim — Department of Electrical and Computer Engineering, The Ohio State University, Columbus, Ohio 43210, United States; orcid.org/0000-0002-1313-7095

Benthara Hewage Dinushi Jayatunga – Department of Physics, Case Western Reserve University, Cleveland, Ohio 44106, United States

Kaitian Zhang — Department of Electrical and Computer Engineering, The Ohio State University, Columbus, Ohio 43210, United States

Menglin Zhu — Department of Materials Science and Engineering, The Ohio State University, Columbus, Ohio 43210, United States

Jinwoo Hwang – Department of Materials Science and Engineering, The Ohio State University, Columbus, Ohio 43210, United States

Kathleen Kash — Department of Physics, Case Western Reserve University, Cleveland, Ohio 44106, United States; orcid.org/0000-0002-6126-7302

Complete contact information is available at: https://pubs.acs.org/10.1021/acs.cgd.1c00630

Notes

The authors declare no competing financial interest. Data Availability: The data that support the findings of this study are available from the corresponding author upon reasonable request.

ACKNOWLEDGMENTS

The authors acknowledge funding support from the U.S. Department of Energy (DE-EE0008718) and the National Science Foundation (DMREF-SusChEM-1533957). Karim, Zhao, Zhu, and Hwang also acknowledge support from the Seed Grant from the Institute for Materials Research at the Ohio State University and the Center for Emergent Materials, an NSF-funded MRSEC under award DMR-1420451. Zhu and Hwang also acknowledge partial support from an NSF-MRSEC, DMR-2011876. Electron microscopy was performed at the Center for Electron Microscopy and Analysis at the Ohio State University.

REFERENCES

- (1) DOE BTO SSL Program. 2018 Solid-State Lighting R&D Opportunities; Brodrick, J., Ed., 2019.
- (2) Krames, M. R. 6-1: Invited Paper: Status and Future Prospects for Visible-Spectrum Light-Emitting Diodes. SID Symposium Digest of Technical Papers, 2016; Vol. 47, pp 39–41.
- (3) Damilano, B.; Gil, B. Yellow-red emission from (Ga,In)N heterostructures. J. Phys. D: Appl. Phys. 2015, 48, 403001.
- (4) Auf der Maur, M.; Pecchia, A.; Penazzi, G.; Rodrigues, W.; Di Carlo, A. Efficiency drop in green InGaN/GaN light emitting diodes: The role of random alloy fluctuations. *Phys. Rev. Lett.* **2016**, *116*, 027401.
- (5) Li, H.; Zhang, H.; Song, J.; Li, P.; Nakamura, S.; DenBaars, S. P. Toward heteroepitaxially grown semipolar GaN laser diodes under electrically injected continuous-wave mode: From materials to lasers. *Appl. Phys. Rev.* **2020**, *7*, 041318.
- (6) Schmidt, M. C.; Kim, K.-C.; Farrell, R. M.; Feezell, D. F.; Cohen, D. A.; Saito, M.; Fujito, K.; Speck, J. S.; DenBaars, S. P.; Nakamura, S. Demonstration of Nonpolarm-Plane InGaN/GaN Laser Diodes. *Jpn. J. Appl. Phys.* **2007**, *46*, L190.
- (7) Farrell, R. M.; Feezell, D. F.; Schmidt, M. C.; Haeger, D. A.; Kelchner, K. M.; Iso, K.; Yamada, H.; Saito, M.; Fujito, K.; Cohen, D. A. Continuous-wave Operation of AlGaN-cladding-free Nonpolar m-Plane InGaN/GaN Laser Diodes. *Jpn. J. Appl. Phys.* **2007**, *46*, L761.
- (8) Zhao, H.; Liu, G.; Zhang, J.; Poplawsky, J. D.; Dierolf, V.; Tansu, N. Approaches for high internal quantum efficiency green InGaN light-emitting diodes with large overlap quantum wells. *Opt. Express* **2011**, *19*, A991–A1007.
- (9) Arif, R. A.; Zhao, H.; Ee, Y.-K.; Tansu, N. Spontaneous emission and characteristics of staggered InGaN quantum-well light-emitting diodes. *IEEE J. Quantum Electron.* **2008**, *44*, 573–580.
- (10) Arif, R. A.; Ee, Y.-K.; Tansu, N. Polarization engineering via staggered InGaN quantum wells for radiative efficiency enhancement of light emitting diodes. *Appl. Phys. Lett.* **2007**, *91*, 091110.
- (11) Hongping Zhao, H.; Arif, R. A.; Tansu, N. Design Analysis of Staggered InGaN Quantum Wells Light-Emitting Diodes at 500-540 nm. *IEEE J. Sel. Top. Quantum Electron.* **2009**, *15*, 1104–1114.
- (12) Park, S.-H.; Ahn, D.; Kim, J.-W. High-efficiency staggered 530 nm InGaN/InGaN/GaN quantum-well light-emitting diodes. *Appl. Phys. Lett.* **2009**, *94*, 041109.
- (13) Zhao, H.; Arif, R. A.; Ee, Y.-K.; Tansu, N. Self-Consistent Analysis of Strain-Compensated InGaN-AlGaN Quantum Wells for Lasers and Light-Emitting Diodes. *IEEE J. Quantum Electron.* **2009**, 45, 66–78.
- (14) Zhao, H.; Arif, R. A.; Ee, Y.-K.; Tansu, N. Optical gain analysis of strain-compensated InGaN-AlGaN quantum well active regions for lasers emitting at 420-500 nm. *Opt. Quantum Electron.* **2008**, *40*, 301–306.
- (15) Zhao, H.; Liu, G.; Tansu, N. Analysis of InGaN-delta-InN quantum wells for light-emitting diodes. *Appl. Phys. Lett.* **2010**, *97*, 131114.
- (16) Arif, R. A.; Zhao, H.; Tansu, N. Type-II InGaN-GaNAs quantum wells for lasers applications. *Appl. Phys. Lett.* **2008**, 92, 011104.
- (17) Park, S.-H.; Lee, Y.-T.; Park, J. Optical properties of type-II InGaN/GaAsN/GaN quantum wells. *Opt. Quantum Electron.* **20092009**, 41, 779–785.
- (18) Han, L.; Kash, K.; Zhao, H. Designs of blue and green light-emitting diodes based on type-II InGaN-ZnGeN₂ quantum wells. *J. Appl. Phys.* **2016**, *120*, 103102.
- (19) Karim, M. R.; Zhao, H. Design of InGaN-ZnSnN2 quantum wells for high-efficiency amber light emitting diodes. *J. Appl. Phys.* **2018**, *124*, 034303.
- (20) Fu, H.; Goodrich, J. C.; Ogidi-Ekoko, O.; Tansu, N. Type-II AlInN/ZnGeN2 quantum wells for ultraviolet laser diodes. *J. Appl. Phys.* **2019**, *126*, 133103.
- (21) Punya, A.; Lambrecht, W. R. L.; Van Schilfgaarde, M. Quasiparticle band structure of Zn-IV-N₂ compounds. *Phys. Rev. B: Condens. Matter Mater. Phys.* **2011**, 84, 165204.

- (22) Blanton, E. W.; He, K.; Shan, J.; Kash, K. Characterization and control of ZnGeN₂ cation lattice ordering. *J. Cryst. Growth* **2017**, *461*, 38–45.
- (23) Zhu, L. D.; Maruska, P. H.; Norris, P. E.; Yip, W.; Bouthillette, L. O. Epitaxial growth and structural characterization of single crystalline ZnGeN₂. MRS Internet J. Nitride Semicond. Res. **1999**, 4, 149–154.
- (24) Tellekamp, M. B.; Melamed, C. L.; Norman, A. G.; Tamboli, A. Heteroepitaxial Integration of ZnGeN2 on GaN Buffers Using Molecular Beam Epitaxy. *Cryst. Growth Des.* **2020**, *20*, 1868–1875.
- (25) Punya, A.; Lambrecht, W. R. L. Band offsets between ZnGeN₂, GaN, ZnO, and ZnSnN₂ and their potential impact for solar cells. *Phys. Rev. B: Condens. Matter Mater. Phys.* **2013**, 88, 075302.
- (26) Jaroenjittichai, A. P.; Lyu, S.; Lambrecht, W. R. L. Erratum: Band offsets between ZnGeN₂, GaN, ZnO, and ZnSnN₂ and their potential impact for solar cells [Phys. Rev. B 88, 075302 (2013)]. *Phys. Rev. B* 2017, 96, 079907.
- (27) Karim, M. R.; Noesges, B. A.; Jayatunga, B. H. D.; Zhu, M.; Hwang, J.; Lambrecht, W. R. L.; Brillson, L. J.; Kash, K.; Zhao, H. Experimental determination of the valence band offsets of ZnGeN2 and (ZnGe)0.94Ga0.12N2 with GaN. J. Phys. D: Appl. Phys. 2021, 54, 245102.
- (28) Karim, M. R.; Jayatunga, B. H. D.; Zhu, M.; Lalk, R. A.; Licata, O.; Mazumder, B.; Hwang, J.; Kash, K.; Zhao, H. Effects of cation stoichiometry on surface morphology and crystallinity of ZnGeN2 films grown on GaN by metalorganic chemical vapor deposition. *AIP Adv.* **2020**, *10*, 065302.
- (29) Karim, M. R.; Jayatunga, B. H. D.; Feng, Z.; Kash, K.; Zhao, H. Metal-Organic Chemical Vapor Deposition Growth of ZnGeN2 Films on Sapphire. *Cryst. Growth Des.* **2019**, *19*, 4661–4666.
- (30) Vickers, M. E.; Kappers, M. J.; Smeeton, T. M.; Thrush, E. J.; Barnard, J. S.; Humphreys, C. J. Determination of the indium content and layer thicknesses in InGaN/GaN quantum wells by x-ray scattering. *J. Appl. Phys.* **2003**, *94*, 1565.
- (31) Nakamura, S. Zn-doped InGaN growth and InGaN/AlGaN double-heterostructure blue-light-emitting diodes. *J. Cryst. Growth* **1994**, *145*, 911–917.
- (32) Eliseev, P. G.; Smagley, V. A.; Perlin, P.; Sartori, P.; Osinski, M. Analysis of impurity-related blue emission in Zn-doped GaN/InGaN/AlGaN double heterostructure. *Proceedings SPIE 2693, Physics and Simulation of Optoelectronic Devices IV*: San Jose, CA, USA, 1996.
- (33) Reshchikov, M. A.; Morkoς, H. Luminescence properties of defects in GaN. J. Appl. Phys. 2005, 97, 061301.
- (34) Grgat, J.; Han, L.; Zhao, H. Analysis of position and thickness dependence of ZnGeN₂ layer in type-II InGaN-ZnGeN2 quantum wells light-emitting diodes. *Conference on Lasers and Electro-Optics, OSA Technical Digest (online) paper STh3I.5*; Optical Society of America, 2017: San Jose, California United States, 2017.